Journal of Cerebral Blood Flow & Metabolism (2010) 30, 1329–1342

www.jcbfm.com

Absolute arterial cerebral blood volume quantification using inflow vascular-space-occupancy with dynamic subtraction magnetic resonance imaging

Manus J Donahue[1], Ediri Sideso[2], Bradley J MacIntosh[1], James Kennedy[2], Ashok Handa[3] and Peter Jezzard[1]

[1]*Department of Clinical Neurology, FMRIB Centre, University of Oxford, Oxford, UK;* [2]*Nuffield Department of Clinical Medicine, University of Oxford, Oxford, UK;* [3]*Nuffield Department of Surgery, University of Oxford, Oxford, UK*

In patients with steno-occlusive disease of the internal carotid artery (ICA), cerebral blood flow may be maintained by autoregulatory increases in arterial cerebral blood volume (aCBV). Therefore, characterizing aCBV may be useful for understanding hemodynamic compensation strategies. A new 'inflow vascular-space-occupancy with dynamic subtraction (iVASO-DS)' MRI approach is presented where aCBV (mL blood/100 mL parenchyma) is quantified without contrast agents using the difference between images with and without inflowing blood water signal. The iVASO-DS contrast mechanism is investigated (3.0 T, spatial resolution = 2.4×2.4×5 mm^3) in healthy volunteers ($n = 8$; age = 29 ± 5 years), and patients with mild ($n = 7$; age = 72 ± 8 years) and severe ($n = 10$; age = 73 ± 8 years) ICA stenoses. aCBV was quantified in right and left hemispheres in controls, and, alongside industry standard dynamic susceptibility contrast (DSC), contralateral (cont), and ipsilateral (ips) to maximum stenosis in patients. iVASO contrast significantly correlated ($R = 0.67$, $P < 0.01$) with DSC-CBV after accounting for transit time discrepancies. Gray matter aCBV (mL/100 mL) was 1.60 ± 0.10 (right) versus 1.61 ± 0.20 (left) in controls, 1.59 ± 0.38 (cont) and 1.65 ± 0.37 (ips) in mild stenosis patients, and 1.72 ± 0.18 (cont) and 1.58 ± 0.20 (ips) in severe stenosis patients. aCBV was asymmetric ($P < 0.01$) in 41% of patients whereas no asymmetry was found in any control. The potential of iVASO-DS for autoregulation studies is discussed in the context of existing hemodynamic literature.
Journal of Cerebral Blood Flow & Metabolism (2010) **30,** 1329–1342; doi:10.1038/jcbfm.2010.16; published online 10 February 2010

Keywords: ASL; cerebral blood flow; cerebral blood volume; MRI; stenosis; VASO

Introduction

Arterial dilation is facilitated by microvascular smooth muscle cells and is closely linked to cerebral blood flow (CBF) regulation (Hillman *et al*, 2007; Rapela and Green, 1964). Autoregulatory increases in arterial cerebral blood volume (aCBV) may have a role in maintaining sufficient CBF in patients with reduced cerebral perfusion pressure and early-stage steno-occlusive disease of the internal carotid artery (ICA) (Boysen, 1973; Derdeyn *et al*, 2002). In such patients, alterations in aCBV may precede alterations in CBF or oxygen extraction fraction and could provide an early indication of hemodynamic impairment and possible stroke risk (Derdeyn *et al*, 2002). However, such autoregulatory effects are not always detectable with current imaging techniques (Schumann *et al*, 1998; Zaharchuk *et al*, 1999) and it is unclear how aCBV should be interpreted for clinical management of patients with ICA steno-occlusive disease.

Total CBV quantification in humans is possible using invasive contrast agents and MRI (Ostergaard *et al*, 1998; Villringer *et al*, 1988), positron emission tomography (Powers and Raichle, 1985), computed tomography (Steiger *et al*, 1993) and single photon emission computed tomography (Sakai *et al*, 1985).

Correspondence: Dr MJ Donahue, Department of Clinical Neurology, FMRIB Centre, University of Oxford, John Radcliffe Hospital, Headington, Oxford OX3 9DU, UK.
E-mail: manus.donahue@clneuro.ox.ac.uk
Received 9 September 2009; revised 15 January 2010; accepted 20 January 2010; published online 10 February 2010

However, noninvasive approaches for measuring CBV in humans would be useful for performing longitudinal studies of CBV regulation and for patients with contraindications to contrast agents. Noninvasive MRI approaches for measuring total (Lu *et al*, 2003) and venous (Stefanovic and Pike, 2005) CBV response to neuronal stimulation have been proposed and arterial spin labeling (ASL) MRI approaches have been modified to allow for aCBV estimation by comparing images with and without gradient-induced dephasing of blood water (Kim and Kim, 2005; Petersen *et al*, 2006). Spin labeling approaches can provide reproducible (Petersen *et al*, 2009) and comparable results to contrast agent-based techniques (Knutsson *et al*, 2010) and have promise for clinical imaging of steno-occlusive disease (Hendrikse *et al*, 2004).

Here, we introduce a modification to the recently proposed inflow vascular-space-occupancy (iVASO) MRI approach (Hua *et al*, 2009*a*) that enables quantification of aCBV in units of mL blood/100 mL parenchyma. This proposed 'iVASO with dynamic subtraction' (iVASO-DS) sequence is similar to spin labeling approaches and involves subtraction of images with and without signal contribution from inflowing blood water. However, here we use the VASO principle of longitudinal blood water magnetization nulling to generate the aCBV-weighted contrast. The purpose of this study is threefold: (1) to present the iVASO-DS theory and show the contrast mechanism in healthy volunteers, (2) to apply this approach to patients with stenotic artery disease and to compare iVASO-DS with industry standard dynamic susceptibility contrast (DSC) CBV imaging, and (3) to assess the potential and limitations of the technique in the clinical context of patients with vascular disease. This work has been previously partially published in abstract form (Donahue *et al*, 2009*c*).

Materials and methods

Measuring CBV Changes With VASO MRI

VASO MRI has been used to measure CBV adjustments associated with increased neuronal activity (Lu *et al*, 2003). In VASO, blood water signal is nulled and the resulting image is anticipated to contain signal only from extravascular tissue. Reductions in the measured tissue signal are then used to quantify increases in the vascular compartment volume that accompanies neuronal activity. The VASO contrast mechanism has been investigated and information regarding signal changes (Donahue *et al*, 2006; Gu *et al*, 2006; Scouten and Constable, 2008), cerebrospinal fluid (CSF) contamination (Scouten and Constable, 2008), consistency with other CBV-weighted (CBVw) approaches (Jin and Kim, 2006), blood inflow (Donahue *et al*, 2009*b*), blood T_1 variation (Donahue *et al*, 2009*d*; Wu *et al*, 2007), and clinical feasibility (Donahue *et al*, 2008; Uh *et al*, 2009) has been investigated.

One limitation of VASO is that the contrast mechanism is generally not designed to measure CBV in absolute units. Instead, VASO is used for assessing relative changes in CBV in response to neuronal tasks. This significantly limits the clinical potential of VASO and therefore it is desirable to extend the VASO approach for absolute CBV determination.

iVASO-DS Pulse Sequence

Recently, a modification has been introduced to the VASO sequence in which only blood water below the imaging volume is nulled. This iVASO approach increases the signal-to-noise ratio (SNR) over conventional VASO and is primarily sensitive to aCBV adjustments (Hua *et al*, 2009*a*). We propose an additional improvement to the iVASO technique to allow absolute aCBV to be quantified. This approach, termed iVASO with dynamic subtraction (iVASO-DS), uses the difference between a consecutively acquired *control* (tissue + blood signal) and *null* (tissue signal only) image (Figure 1A).

Null Acquisition: The null acquisition is in principle equivalent to iVASO, whereby inflowing blood water signal is nulled and the tissue signal in the imaging slice is unaltered. To accomplish this, a nonselective adiabatic radiofrequency (RF) inversion pulse is applied ($RF = 180_y^{ns}$), which is immediately followed by a slice-selective inversion of the imaging slice ($RF = 180_y^{ss}$). Therefore, blood water outside the imaging slice is inverted whereas blood water within the imaging slice is unaltered. After an inversion time (TI), an image is acquired. The TI is chosen to correspond to the time when the longitudinal magnetization (M_z) of inflowing blood water is zero.

Control Acquisition: The inflowing blood water is not inverted, and is therefore nonzero, and the tissue signal is prepared identically to the case of the *null acquisition*. This is accomplished by applying two consecutive slice-selective adiabatic inversion pulses ($RF = 180_y^{ss} + 180_y^{ss}$) followed by the same TI as in the *null acquisition*. Therefore, the water signal within *and* outside the slice is unaltered by the RF preparation.

Difference Image: The tissue magnetization is identical in both *control* and *null* images, whereas the inflowing blood water is zero in only the *null* image (Figure 1B). A subtraction, *control*−*null*, gives a CBVw map.

The subtraction procedure is similar to the increasingly used CBF-weighted ASL experiment, except that instead of tagging the blood, as is performed in ASL, blood water signal is nulled by choosing the TI to correspond to the blood water null time. Therefore, the iVASO-DS sequence is a combination of ASL and iVASO. Furthermore, as the TI needed for blood nulling is approximately on the order of the expected arterial-to-capillary transit times (700 to 1,100 ms), the CBV sensitivity is precapillary (as any tissue or venous contribution would require an additional transit time of 500 to 2,000 ms).

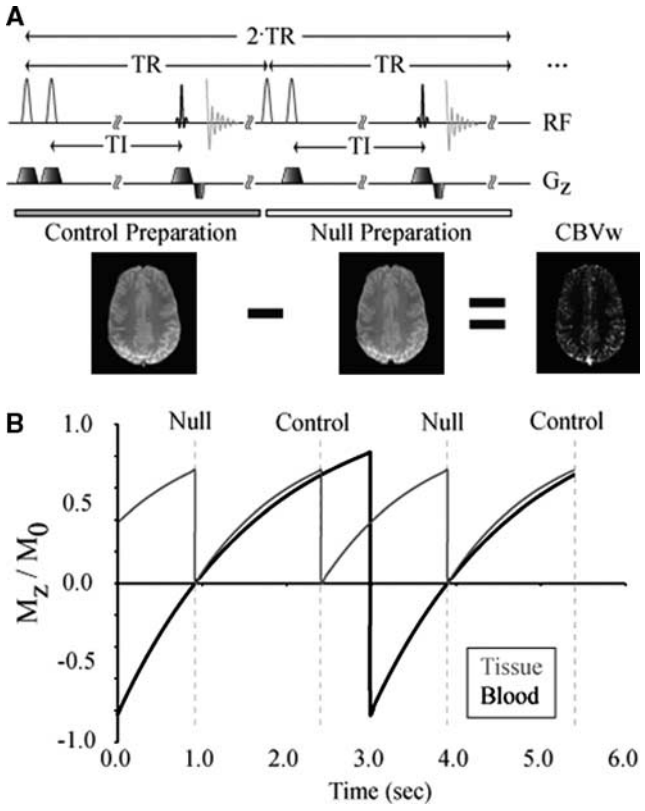

Figure 1 (**A**) The inflow VASO with dynamic subtraction (iVASO-DS) pulse sequence. In the control preparation, two slice selective adiabatic inversion pulses are sequentially applied, followed by an inversion time (TI), and finally a 2D single-shot echo planar image gradient echo acquisition. In the control preparation, both blood and tissue magnetization are nonzero. After the control preparation, a null preparation is applied in which a nonselective adiabatic inversion is immediately followed by a slice-selective inversion (tissue 'flip back'). The same TI is allowed, which corresponds to the time for the blood water magnetization to recover to zero. Control—null yields a CBVw map. (**B**) A snapshot in time of the tissue (gray) and inflowing blood (black) magnetization. This simulation has been performed for a representative TR/TI = 1,492/914 ms. Note that tissue magnetization is only influenced by the readout excitation pulses, whereas the inflowing blood water magnetization is only influenced by an inversion pulse in alternate TRs.

aCBV Quantification

The total gray matter (GM) parenchyma signal ($S_{\mathrm{GM,par}}$) in a voxel is the sum of signal from extravascular tissue ($S_{\mathrm{GM},t}$) and blood (S_b). Parenchymal signal in the *control* ($S^C_{\mathrm{GM,par}}$) and *null* ($S^N_{\mathrm{GM,par}}$) iVASO-DS acquisition is therefore:

$$S^C_{\mathrm{GM,par}} = A \cdot (S^C_{\mathrm{GM},t} + S^C_b) \quad (1)$$

and

$$S^N_{\mathrm{GM,par}} = A \cdot S^N_{\mathrm{GM},t} \quad (2)$$

where A is a constant that depends on the scanner gain and image scaling.

Tissue signal is ideally identical in the *null* and *control* acquisitions in the present implementation (Figure 1A). The difference signal (ΔS) should be simply the blood signal in the control acquisition, modified by any possible residual signal owing to imperfect static tissue signal cancelling:

$$\Delta S = S^C_{\mathrm{GM,par}} - S^N_{\mathrm{GM,par}} = A \cdot [S^C_b + (\beta^C - \beta^N) S_{\mathrm{GM},t}] \quad (3)$$

The β terms in equation (3) have been introduced to account for possible imperfect tissue flip back efficiency (with $\beta^C = S^C_{\mathrm{GM},t}/S_{\mathrm{GM},t}$ and $\beta^N = S^N_{\mathrm{GM},t}/S_{\mathrm{GM},t}$) that may lead to imperfect static tissue signal cancellation, for example as a result of slice profile effects or differential magnetization transfer contributions. As the same adiabatic pulse was used in the control ($\mathrm{RF} = 180_y^{ss} + 180_y^{ss}$) and null ($\mathrm{RF} = 180_y^{ns} + 180_y^{ss}$) acquisitions, it is likely that any inefficiencies in tissue inversion and flip back will be similar between scans (i.e., $\beta^C \approx \beta^N$).

The blood water signal can be expanded in terms of the blood water density, aCBV (units = mL blood/100 mL parenchyma), longitudinal blood water magnetization (M_b), echo time (TE), time for the labeled blood water bolus to reach the capillaries (capillary arrival time: τ), the blood water density ($C_b \approx 0.87$ mL/mL (Herscovitch and Raichle, 1985)), and effective blood water relaxation rate ($R^*_{2,\mathrm{b}} \approx 16\ \mathrm{secs}^{-1}$ (Zhao *et al*, 2007)):

$$S^i_b = C_b \cdot \mathrm{aCBV} \cdot \frac{\mathrm{TI}}{\tau} \cdot M^i_b(\mathrm{TI},\ \mathrm{TR}) \cdot e^{-\mathrm{TE} \cdot R^*_{2,b}} \quad i = C \text{ or } N \quad (4)$$

TI/τ is approximately the fraction of blood present in the arterial compartment and assumes that blood from the labeling bolus begins arriving in the imaging slice immediately (see Discussion). The steady-state M_b depends on TI and repetition time (TR). As the nonselective inversion pulse is only applied in *null* acquisitions, twice the TR must be used in determining the optimal TI and TR combination to keep inflowing blood water nulled during this period:

$$M^N_b(\mathrm{TI},\mathrm{TR}) = M_{0,b} \cdot \left(1 - 2 \cdot e^{-\frac{\mathrm{TI}}{T_{1,b}}} + e^{-\frac{2 \cdot \mathrm{TR}}{T_{1,b}}}\right) = 0 \quad (5)$$

During the control acquisitions inflowing blood water magnetization is given by

$$M^C_b(\mathrm{TI},\mathrm{TR}) = M_{0,b} \cdot \left(1 - 2 \cdot e^{-\frac{\mathrm{TI}+\mathrm{TR}}{T_{1,b}}} + e^{-\frac{2 \cdot \mathrm{TR}}{T_{1,b}}}\right) \quad (6)$$

By choosing TI and TR such that equation (5) is satisfied, it is possible to obtain the null weighting desired. Table 1 shows different TR and TI combinations that satisfy this constraint for a 3.0 T arterial $T_{1,b} = 1{,}725$ ms (Lu *et al*, 2004).

Using equations (3 to 6), aCBV can be quantified from ΔS:

$$\mathrm{aCBV} = \frac{\Delta S - A \cdot \Delta\beta \cdot S_{\mathrm{GM},t}}{A \cdot C_b \cdot \frac{\mathrm{TI}}{\tau} \cdot M^C_b(\mathrm{TI},\mathrm{TR})} \cdot e^{\mathrm{TE} \cdot R^*_{2,b}} \quad (7)$$

The remaining unknowns are the scaling factor A and $M_{0,b}$, which can both be calculated from signal in the absence of the iVASO-DS preparation pulses, and the $\Delta\beta = \beta^C - \beta^N$ term is related to any possible residual signal that remains after subtraction and is due to imperfect tissue signal cancellation.

Table 1 Methodological study

TR (ms)	*TI (ms)*	$M_{GM,t}$	M_b^C	M_b^N
250	232	0.19	0.24	0.0
500	429	0.34	0.39	0.0
1,000	725	0.57	0.58	0.0
2,000	1,034	0.81	0.75	0.0
3,000	1,143	0.92	0.85	0.0
4,000	1,179	0.96	0.91	0.0
5,000	1,190	0.98	0.95	0.0
6,000	1,194	0.99	0.97	0.0
7,000	1,195	1.0	0.98	0.0
8,000	1,196	1.0	0.99	0.0
446	389	0.31	0.36	0.0
550	464	0.37	0.42	0.0
664	539	0.42	0.47	0.0
788	614	0.48	0.51	0.0
927	689	0.54	0.56	0.0
1,085	764	0.60	0.60	0.0
1,269	839	0.63	0.64	0.0
1,492	914	0.71	0.68	0.0
1,778	989	0.77	0.73	0.0
2,186	1,064	0.84	0.78	0.0

TR/TI combinations, residual tissue magnetization ($M_{GM,t}$), control (M_b^C), and nulled (M_b^N) blood magnetization. The upper half of the table shows the values over a typical range of VASO TRs, whereas the lower half shows the values more closely centered on the range of capillary arrival times and measured in the *methodological experiment*.

Calculating A and $M_{0,b}$

There are several ways of calculating A and $M_{0,b}$ (Petersen *et al*, 2006). Here, parenchymal white matter (WM) signal is measured in an image in the absence of the iVASO-DS preparation pulses. As WM does not partial volume with CSF and the WM blood fraction is estimated to be small (about 1%), the WM signal can be approximated:

$$S_{\mathrm{WM,\,par}} = A \cdot C_{\mathrm{WM}} \cdot M_{\mathrm{WM}}(\mathrm{TI},\mathrm{TR}) \cdot e^{-\mathrm{TE}\cdot R^*_{2,WM}} \qquad (8)$$

where A is the same scaling constant as above, $C_{\mathrm{WM}} \approx 0.73$ mL/mL (Herscovitch and Raichle, 1985) is the WM water density, M_{WM}(TI,TR) is the longitudinal magnetization for WM, and $R^*_{2,\mathrm{WM}} \approx 30\,\mathrm{secs}^{-1}$ (measured here) is the WM effective transverse relaxation rate. In the absence of iVASO-DS preparation, saturation recovery is given by

$$M_{\mathrm{WM}}(\mathrm{TI},\mathrm{TR}) = M_{0,\mathrm{WM}} \cdot \left(1 - e^{-\frac{\mathrm{TR}}{T_{1,\mathrm{WM}}}}\right) \qquad (9)$$

where $T_{1,\mathrm{WM}} \approx 800$ ms is the longitudinal relaxation time of WM at 3.0 T. Finally, it is possible to relate the equilibrium magnetization between WM and blood water through the WM blood–brain barrier partition coefficient (Herscovitch and Raichle, 1985):

$$\frac{M_{0,\mathrm{WM}}}{M_{0,b}} \approx \frac{C_{\mathrm{WM}}}{C_b} = \lambda_{\mathrm{WM}} \approx 0.82\,\mathrm{mL/g} \qquad (10)$$

Incorporating equation (9):

$$A \cdot M_{0,\mathrm{WM}} = A \cdot M_{0,b} \cdot \lambda_{\mathrm{WM}} = \frac{S_{\mathrm{WM,\,par}}}{C_{\mathrm{WM}} \cdot \left(1 - e^{-\frac{TR}{T_{1,\mathrm{WM}}}}\right)} \cdot e^{\mathrm{TE}\cdot R^*_{2,\mathrm{WM}}} \qquad (11)$$

Estimating Residual Tissue Signal

The residual tissue signal owing to differences in flip back efficiency in control and null acquisitions was measured by performing short TI = 389 ms iVASO-DS experiments and recording residual WM signal ($\Delta S_{\mathrm{resid}}$) in the difference image. At this short TI, it is anticipated that the blood contribution to WM signal, $S_{\mathrm{WM,par}}$, will be zero and any remaining signal difference will be due to inefficiencies in tissue signal cancellation. This is expected because (1) WM aCBV is small (< 0.5%) and (2) WM capillary arrival times are much longer than TI. Therefore, at short TI, the blood contribution to the iVASO-DS contrast in WM is expected to be negligible, and any residual signal is likely because of imperfect tissue signal cancellation. Specifically,

$$\Delta\beta = \frac{\Delta S_{\mathrm{resid}}}{A \cdot S_{\mathrm{WM.\,par}}} \qquad (12)$$

where $S_{\mathrm{WM,par}}$ is given by equation (8).

Experiment

All study participants provided informed, written consent in accordance with the Oxfordshire Research Ethics Committee. Three separate sets of experiments were conducted to understand the nature of the iVASO-DS contrast mechanism. First, a *methodological experiment* was performed in healthy volunteers ($n = 5$; age = 27 ± 3 years) where iVASO-DS images were acquired over a range of TI values. As with ASL, iVASO-DS contrast will be sensitive to choice of TI and we sought to understand how CBV values are influenced by this choice. Second, a *healthy control experiment* was performed in which aCBV was quantified in a population of healthy volunteers ($n = 8$; age = 28 ± 5 years) using optimal imaging parameters from the methodological study. Third, a *steno-occlusive disease experiment* was performed in which the same imaging parameters from the healthy control experiment were applied in a group of patients with duplex-ultrasound confirmed severe steno-occlusive disease of the ICA (stenosis ≥ 70%; $n = 9$; age = 73 ± 8 years). Values from these patients were compared against aCBV values from the *healthy control experiment* (stenosis ≈ 0%) and also against age-matched individuals with mild (15% ≤ stenosis < 70%; $n = 8$; 72 ± 8 years). All patients were recruited from a regional vascular duplex scanning laboratory. There was a varied referral pattern ranging from a dedicated daily transient ischemic attack clinic to in-hospital referrals. Patients with occlusion were identified from a vascular studies database and invited to participate in the study. One patient in the severe stenosis category had a previous ischemic stroke. Volunteers in the healthy control experiment did not undergo duplex-ultrasound screening, however, were assumed to have insignificant stenosis burden given their lack of symptoms, age (28 ± 5 years) and general good health. In the steno-occlusive disease study, DSC data were obtained from patients for the purpose of comparing the iVASO-DS aCBV values with industry standard DSC CBV.

Experiments were performed at 3.0 T (Siemens, Erlangen, Germany). Common iVASO-DS experimental para-

meters for all experiments were FOV = 240 × 240 mm², spatial resolution = 2.4 × 2.4 × 5 mm³, body coil transmit, 12-channel head coil receive, parallel imaging using GeneRalized Autocalibrating Partially Parallel Acquisitions (GRAPPA) (Griswold *et al*, 2002) with acceleration factor = 2.0, TE = 18 ms, gradient echo single-shot echo planar image, 1 slice (flip angle = 90°) centered 5 mm above the top of the corpus callosum with anterior commissure-posterior commissure orientation, and 10 difference image averages. In all experiments, an inversion recovery image (TR/TI = 5,000/1,054 ms) with identical spatial resolution and readout as the iVASO-DS acquisition was used for purposes of generating a GM mask.

Methodological Experiment: Ten TR and TI combinations were investigated to understand how the iVASO-DS contrast was influenced by inflow time. The TI choices were chosen in 75 ms increments to span the approximate range of known capillary arrival times (389 to 1,064 ms); values are shown in Table 1 (lower). TR was adjusted for each TI to keep $M_b^N(\mathrm{TI},\ \mathrm{TR}) = 0$. The short TI = 389 ms acquisition was used for assessing flip back efficiency. An arterial time-of-flight (TOF) acquisition was obtained to qualitatively compare the location of arteries with the iVASO-DS maps. TOF scan parameters were TR/TE = 22/4.3 ms, spatial resolution = 0.75 × 0.75 × 1 mm³.

Healthy Control Experiment: On the basis of the results of the *methodological study,* a single TR/TI combination of 1,778/989 ms was chosen. This TI was deemed to be long enough to allow for blood water in the imaging slice to begin to reach capillaries, yet not long enough to introduce substantial exchange between blood and tissue water.

Steno-Occlusive Disease Experiment: The same TR/TI combination and iVASO-DS parameters as in the *healthy control experiment* were used. Additionally, diffusion weighted imaging (DWI) was performed (22 slices, TR/TE = 4,400/93 ms, spatial resolution = 1.6 × 1.6 × 3.0 mm³, b = 1,000 secs/mm²) to identify any possible diffusion hyperintensities and DSC with standard gadolinium diethylenetriamine penta-acetic acid injection (22 slices, TR/TE = 1,481/30 ms, spatial resolution = 1.7 × 1.7 × 5 mm³) was used for total CBV, CBF, and mean transit time (MTT) quantification. Imaging parameters for DSC were based on recommendations from the Acute Stroke Research Roadmap (Wintermark *et al*, 2008).

Analysis

First, all data were corrected for motion with Motion Correction using FMRIB's Linear Image Registration Tool (MCFLIRT) (Jenkinson *et al*, 2002). Second, coil sensitivity will vary over the 12-channel head coil and this will introduce a spatial dependence in the A calibration factor. The sensitivity varied by a mean factor of 1.3 from WM where the reference region of interest (ROI) was drawn for the M_0 calibration to the GM ribbon where aCBV quantification was performed. Therefore, the measured S_{WM} was multiplied by a factor of 1.3 to reduce bias in the aCBV, which would be attributable to heterogeneity in coil sensitivity.

A GM mask was overlaid on the iVASO-DS CBV maps. The GM mask was generated from an inversion recovery image with identical spatial resolution and readout modality as the iVASO-DS acquisition. The scalp was removed from the inversion recovery image and a signal intensity threshold, based on a histogram of all values in the image, was used to generate the mask. Only aCBV within this mask was evaluated, according to the above model, separately for left and right hemispheres. For the *healthy control experiment* and *steno-occlusive disease experiment*, TI = 989 ms was used. On the basis of literature values of arterial transit times (Petersen *et al*, 2009), $\mathrm{TI} \approx \tau$ for this choice. Patients were grouped into three categories, those with duplex-ultrasound confirmed asymmetric mild stenosis (15% ≤ stenosis < 70%), asymmetric severe stenosis (stenosis ≥ 70%), and symmetric ICA stenosis (L/R ICA stenosis burden equal). aCBV was then quantified ipsilateral and contralateral to maximum stenosis burden. The two patients who had identical stenosis burdens in left and right ICAs were excluded from any ipsilateral/contralateral comparisions.

For DSC analysis in the steno-occlusive disease experiment, PErfusioN Graphical User Interface (Penguin) software with a singular value decomposition was applied to calculate CBF, CBV, and MTT (www.cfin.au.dk/software). Spatial smoothing (full width half max (FWHM) = 6 mm) was applied to DSC and iVASO-DS data in the steno-occlusive study. DSC quantification is sensitive to arterial input function choice; automated arterial input function detection available in the software was used; all maps are reported in arbitrary units (a.u.) and only contralateral-to-ipsilateral ratios are quantified, separately for DSC-CBF, DSC-CBV, and DSC-MTT. Additionally, we attempt to account for capillary arrival time asymmetries in the iVASO-DS data by using the DSC-measured MTT, which in the absence of collateral flow would be expected to be proportional to flow velocity and hence to the capillary arrival time. Therefore, a new corrected contralateral-to-ipsilateral iVASO-DS ratio was calculated in patients,

$$\left[\frac{\Delta S_{\mathrm{cont}}}{\Delta S_{\mathrm{ips}}}\right]_{\mathrm{corrected}} = \left[\frac{\Delta S_{\mathrm{cont}}}{\Delta S_{\mathrm{ips}}}\right] \cdot \left[\frac{\mathrm{MTT}_{\mathrm{cont}}}{\mathrm{MTT}_{\mathrm{ips}}}\right] \qquad (13)$$

SNR was calculated in the iVASO-DS data as [mean ΔS]/[standard deviation of ΔS over all measurements]. Statistical tests were performed to determine the significance level of signal variation. Hemodynamic values may not necessarily follow a normal distribution and therefore nonparametric permutation testing (Nichols and Holmes, 2002) was used to assess statistical differences between left and right hemisphere aCBV, as well as ipsilateral and contralateral hemisphere aCBV, DSC-CBF, DSC-CBV, and DSC-MTT in the steno-occlusive disease study. Significance was defined as $P < 0.01$. For group comparisons of mean aCBV between healthy volunteers, mild stenosis, and severe stenosis patients, a Student's t-test was used with significance $P < 0.01$.

Results

Figures 2A and 2B show simulations depicting how iVASO-DS is influenced by the capillary arrival time (τ) and aCBV. In Figure 2A, simulated iVASO-DS signal is plotted against a range of τ values assuming a constant aCBV = 1.5 mL/100 mL and TI = 989 ms. This model assumes an infinite blood water tagging volume, which is approximately correct for this range of τ given that the inversion pulse is non-selective. For short τ, the difference signal is large owing to blood having completely filled the vascular compartment at TI. For long τ, the magnetic resonance (MR) signal difference is reduced as

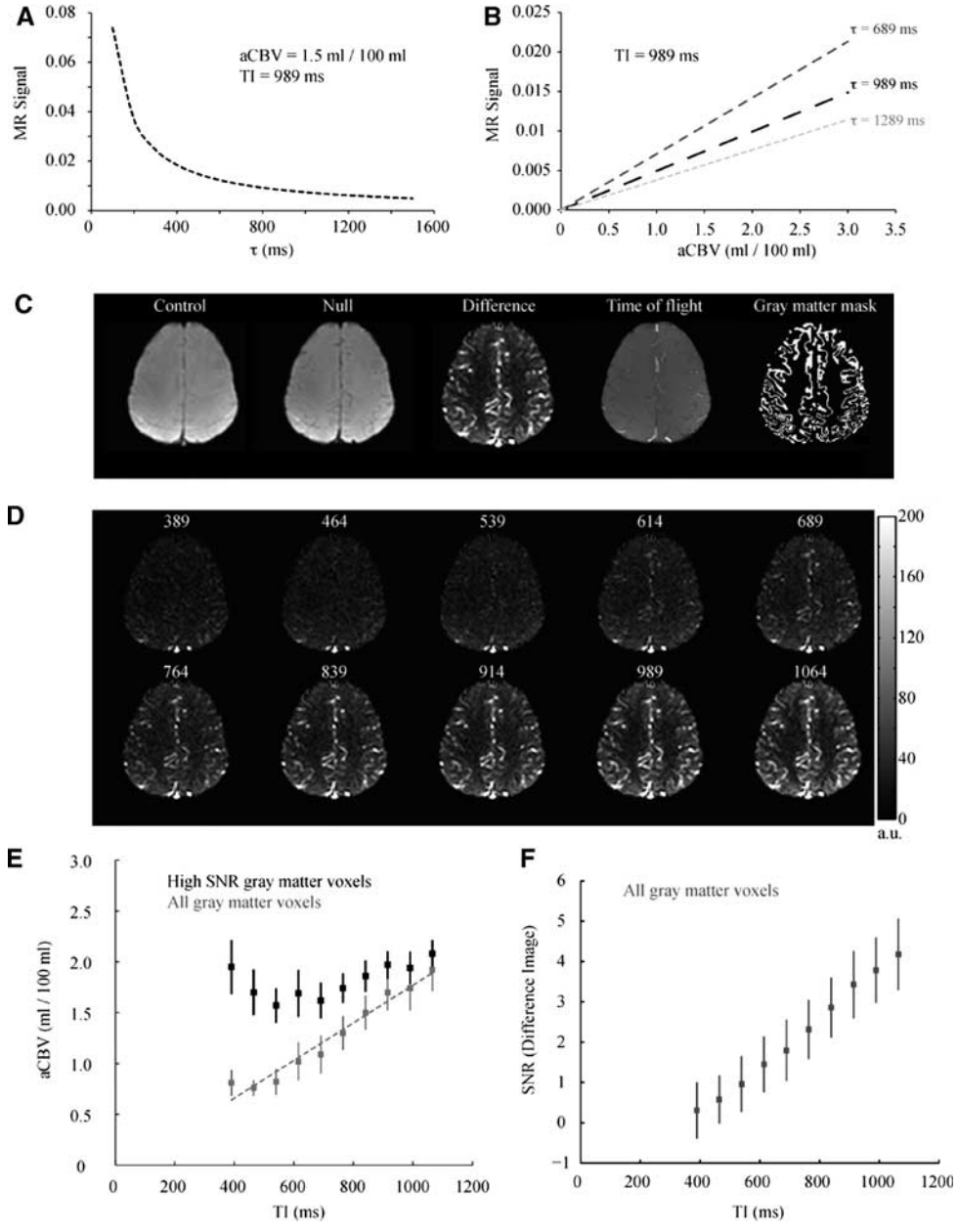

Figure 2 Methodological study. Simulations demonstrating the effect of capillary arrival time (τ) and aCBV on iVASO-DS MR signal. (**A**) iVASO-DS signal versus τ for aCBV = 1.5 mL/100 mL and TI = 989 ms. MR signal is large for short τ but reduces at long τ. (**B**) iVASO-DS signal versus aCBV for three possible τ times. The simulations assume TI = 989 ms. The signal is linear with aCBV, suggesting that an iVASO-DS image alone is proportional to aCBV. (**C**) Left to right: a representative control, null, difference, time-of-flight, and gray matter mask obtained from the *methodological experiment*. Voxels within the GM mask were used for aCBV quantification. (**D**) iVASO-DS CBVw images for varying TI (range 389 to 1,064 ms). The TR was adjusted to keep steady-state blood water nulled (see Table 1). (**E**) Gray matter aCBV as a function of TI. The gray data points represent all GM voxels and the line is the best fit line to these points. The measured aCBV is approximately linear with TI for the approximate range of capillary arrival times. The black data points show the measured aCBV for voxels with high SNR only. (**F**) The SNR of the iVASO-DS difference image as a function of TI.

insufficient time has elapsed for blood to reach capillaries. Figure 2B shows the expected iVASO-DS signal versus aCBV for possible $\tau = 689$, 989, and 1,289 ms. An imaging TI = 989 ms is assumed. Signal is linear with aCBV; the slope increases with decreasing τ. Therefore, for constant τ, the iVASO-DS ΔS is linear with aCBV.

Figures 2C to 2F show the results of the *methodological experiment* in which iVASO-DS contrast was investigated for a range of TI possibilities. In Figure 2C, a representative TI = 989 ms *control*, *null*, and *difference image* are shown (left). The TOF image depicting artery locations and GM mask depicting voxels in which aCBV was quantified are shown on the right. The control and null images effectively look equivalent as the aCBV is only a small fraction ($\sim$1% to 2%) of the total voxel volume. In our implementation, the sagittal sinus vein is also nulled. However, the sagittal sinus is not included in the GM mask and is not expected to bias aCBV results. In Figure 2D, the iVASO-DS difference images are shown for varying TI. For each TI, the TR was varied to keep steady-state blood water signal nulled in the *null* acquisition. The flip back inversion efficiency was estimated from the TI = 389 ms residual WM signal: $\Delta\beta = 0.0164 \pm 0.0018$.

For short TI < 614 ms, signal is predominately uniform, however small hyperintensities can be seen in posterior regions where large vessels are present. For TI $\geq$ 614 ms, blood water from the bolus begins to enter the smaller vessels. The quantified aCBV is shown in Figure 2E for both an ROI containing only voxels with high SNR (black) and within an ROI containing all GM (gray). The SNR threshold was chosen as 1 s.d. below the mean of the SNR in the TI = 1,064 ms image. SNR was 4.2 ± 0.74 ($n = 5$; mean $\pm$ s.d.) in the TI = 1,064 ms image. Within the ROI containing all GM the aCBV is approximately linear with TI. For the ROI containing only high SNR voxels, a different trend is observed. Here, aCBV is increased at short TI, which is due to the increased fractional contribution from voxels containing large vessels, whereas aCBV reduces at intermediate TI and no statistically significant difference ($P > 0.01$) is found for aCBV values above TI = 839 ms. Figure 2F shows mean GM SNR versus TI, which is approximately linear over the TI range studied here.

Table 2 shows the results from the *healthy control experiment.* No statistical variation in aCBV between hemispheres was observed on average ($P = 0.430$) or individually for any healthy volunteer. Mean GM aCBV was found to be 1.60 ± 0.10 mL/100 mL and 1.61 ± 0.20 mL/100 mL in right and left hemispheres, respectively. Note the large variation in aCBV over the GM region (individual aCBV standard deviations), which suggests that aCBV varies considerably between GM voxels. This is not unexpected as voxels at this spatial resolution will partial volume to different extents with small and large vessels.

Table 3 shows the results from the *steno-occlusive disease experiment.* No patients had DWI lesions in the GM mask analyzed. Above, the patient symptoms, reason for scan, and right and left ICA stenosis percentages are shown. Below, aCBV and DSC ratios for the different modalities are shown. Figures 3A to 3C show representative iVASO-DS and DSC-measured CBF, CBV, and MTT maps for three representative patients. These patients correspond to PT8 (A), PT16 (B), and PT6 (C) in Table 3. Note the reasonably good qualitative consistency between iVASO-DS and DSC-CBV, even in the presence of statistically significant MTT asymmetries (Figure 3A). PT8 (A), a patient with 80%/100% right/left ICA stenosis burden and right amaurosis fugax, exhibited a clear MTT asymmetry, which led to an apparent elevated aCBV on the right side. However, when this asymmetry was accounted for (Table 3), the aCBV was not statistically different between hemispheres. PT16 (B), similarly exhibited right amaurosis fugax with only a mild right/left stenosis burden of 35%/35%. This patient had no MTT asymmetry, however did have a statistically elevated aCBV on the right side. PT6 (C) exhibited a mild stenosis 40%/15% (right/left) with symptoms consistent with global amnesia. No asymmetry in any of the imaging modalities is found. Contralateral:ipsilateral iVASO-DS contrast is also compared with DSC-CBV contrast. In the absence of the MTT correction, the ratios exhibit a weak correlation (Figure 3D). When MTT asymmetries are taken into account (Figure 3E), the correlation increases and the trend becomes significant ($P < 0.01$). Figures 3F and 3G show DSC CBF hemispheric values (Figure 3F) and iVASO-DS values (Figure 3G). The CBF values are highly symmetric between hemispheres, whereas the iVASO-DS values are less symmetric. In addition, the smaller slope in the iVASO-DS plot is consistent with higher aCBV contralateral to the side of maximum stenosis burden, which is generally in the symptomatic hemisphere (Table 3) and is consistent with autoregulatory vasodilation. All patient ratios are shown in Table 3 (lower). The comparison between imaging modalities generally exhibit no specific trend for mild stenosis patients,

Table 2 Healthy control study

	Sex	*Age (years)*	*Right aCBV mL/100 mL*	*Left aCBV mL/100 mL*
HV1	M	27	1.67 ± 1.68	1.90 ± 1.90
HV2	M	33	1.35 ± 1.50	1.32 ± 1.35
HV3	M	29	1.50 ± 1.44	1.58 ± 1.54
HV4	F	24	1.62 ± 1.69	1.45 ± 1.41
HV5	F	26	1.70 ± 2.06	1.46 ± 1.44
HV6	M	26	1.69 ± 2.01	1.79 ± 1.79
HV7	F	24	1.66 ± 1.62	1.67 ± 1.74
HV8	M	40	1.58 ± 1.87	1.68 ± 1.75
Mean		$\mathbf{29 \pm 5}$	$\mathbf{1.60 \pm 0.10}$	$\mathbf{1.61 \pm 0.20}$

Right and left aCBV in gray matter for healthy volunteers (HV). Values are mean $\pm$ s.d. of aCBV values over gray matter cortex. No significant differences ($P < 0.01$) between brain hemispheres were found.

Table 3 Steno-occlusive disease study

	Sex	*Age (years)*	*Symptoms*	*Reason for scan*	*Right stenosis (%)*	*Left stenosis (%)*
Mild						
PT1	M	61	TIA. Left facial weakness	TIA	50	55
PT2	M	62	Left facial weakness	Based on symptoms	30	50
PT3	M	71	TIA. Right arm weakness	TIA	40	60
PT4	M	68	Slightly blurred bilateral vision/asymptomatic	Before aortic valve replacement	0	30
PT5	M	83	Left hand weakness and dysphasia	Based on symptoms	60	55
PT6	M	75	Transient global amnesia	Based on symptoms	40	15
PT7	F	80	Right leg weakness	Based on symptoms	60	40
Mean		71 ± 8				
Severe						
PT8	M	75	TIA. Right amaurosis fugax	TIA	80	100
PT9	F	84	Left arm/leg paraesthesia	Previous common carotid artery ligation	15	100
PT10	M	76	Slightly blurred bilateral vision/asymptomatic	Before coronary artery bypass surgery	80	85
PT11	M	76	Left Amaurosis Fugax	Based on symptoms	30	80
PT12	M	62	Asymptomatic	Recommended based on earlier research scan	100	65
PT13	F	68	TIA. Right facial weakness	Based on symptoms	40	80
PT14	F	61	Left arm weakness	Right hemispheric ischemic stroke	100	30
PT15	M	84	Asymptomatic	Reocclusion of previous right CEA	100	80
Mean		73 ± 9				
Symmetric						
PT16	M	74	Right amaurosis fugax	Based on symptoms	35	35
PT17	M	75	Asymptomatic	Left carotid bruit	100	100
Mean		75 ± 1				

	aCBV cont (mL/100 mL)	*aCBV ips (mL/100 mL)*	*aCBV cont/ips*	*CBF cont/ips*	*MTT cont/ips*	*DSC CBV cont/ips*	*MTT-corrected aCBV cont/ips*
Mild							
PT1	1.28 ± 1.00	1.45 ± 1.46	0.88 ± 1.12	1.00 ± 0.65	0.95 ± 0.39	0.94 ± 0.60	0.84 ± 1.12
PT2	1.46 ± 1.33	1.52 ± 1.27	0.96 ± 1.19	0.93 ± 0.52	1.00 ± 0.36	0.95 ± 0.64	0.96 ± 1.24
PT3	1.55 ± 1.20	1.73 ± 1.52	0.90 ± 1.05*	0.85 ± 0.57*	0.95 ± 0.44	0.83 ± 0.68*	0.86 ± 1.08*
PT4	1.23 ± 1.31	1.30 ± 1.45	0.95 ± 1.46	0.85 ± 0.53*	1.05 ± 0.38	0.84 ± 0.62*	0.99 ± 1.57
PT5	2.31 ± 1.45	2.38 ± 1.57	0.97 ± 0.88	0.99 ± 0.60	0.95 ± 0.33	0.96 ± 0.70	0.92 ± 0.90
PT6	1.44 ± 1.10	1.40 ± 1.04	1.03 ± 1.10	1.01 ± 0.57	1.00 ± 0.28	1.01 ± 0.61	1.03 ± 1.13
PT7	1.87 ± 1.84	1.81 ± 1.53	1.03 ± 1.34	1.01 ± 0.68	1.11 ± 0.50*	1.12 ± 0.89	1.15 ± 1.58*
Mean	**1.59 ± 0.38**	**1.65 ± 0.37**	**0.96 ± 0.06**	**0.95 ± 0.07**	**1.00 ± 0.06**	**0.95 ± 0.10**	**0.96 ± 0.11**
Severe							
PT8	1.67 ± 1.73	1.45 ± 1.50	1.15 ± 1.69*	1.23 ± 0.78*	0.83 ± 0.34*	1.01 ± 0.72	0.96 ± 1.46
PT9	1.86 ± 1.64	1.52 ± 1.14	1.22 ± 1.42*	1.25 ± 0.76	0.90 ± 0.38*	1.11 ± 0.77*	1.10 ± 1.35
PT10	1.95 ± 2.65	1.66 ± 2.41	1.17 ± 2.34*	1.10 ± 0.66	1.13 ± 0.61	1.32 ± 1.24	1.33 ± 2.74*
PT11	1.73 ± 2.03	1.96 ± 2.11	0.88 ± 1.41	1.04 ± 0.62	1.01 ± 0.37	1.03 ± 0.80	0.89 ± 1.46
PT12	1.59 ± 1.67	1.62 ± 1.85	0.98 ± 1.52	0.95 ± 0.72*	1.09 ± 0.50*	1.05 ± 0.67*	1.07 ± 1.73*
PT13	1.76 ± 1.86	1.67 ± 1.49	1.05 ± 1.46	0.77 ± 0.54*	1.18 ± 0.54*	0.99 ± 0.68	1.25 ± 1.82*
PT14	1.84 ± 1.50	1.45 ± 1.22	1.27 ± 1.49*	1.19 ± 0.82*	0.92 ± 0.35	1.07 ± 0.87*	1.17 ± 1.44*
PT15	1.37 ± 1.13	1.28 ± 1.02	1.07 ± 1.23*	0.87 ± 0.47	1.06 ± 0.37	0.90 ± 0.66	1.13 ± 1.36*
Mean	1.72 ± 0.18	1.58 ± 0.20	1.10 ± 0.13	1.05 ± 0.17	1.02 ± 0.12	1.06 ± 0.11	1.11 ± 0.14

Symmetric	*aCBV right*	*aCBV left*	*aCBV right/left*	*CBF right/left*	*MTT right/left*	*DSC CBV right/left*	*MTT-corrected aCBV right/left*
PT16	2.46 ± 1.24	2.15 ± 1.31	1.14 ± 0.90*	0.87 ± 0.45*	0.99 ± 0.34	1.02 ± 0.77	1.13 ± 0.97
PT17	1.52 ± 1.12	1.64 ± 1.49	0.93 ± 1.08	0.94 ± 0.59	1.36 ± 0.82*	1.21 ± 0.87	1.26 ± 1.65
Mean	1.99 ± 0.66	1.90 ± 0.36	1.04 ± 0.15	0.91 ± 0.05	1.18 ± 0.26	1.12 ± 0.13	1.20 ± 0.10

TIA, transient ischemic attack.
(Above) patient sex, age, symptoms, reason for scan, and right and left stenoses. Maximum stenosis side is identified as 'ipsilateral,' the opposite side as 'contralateral.' (Below) patient aCBV values (mean ± s.d. over all voxels) and contralateral:ipsilateral ratios for iVASO and DSC. Far right: iVASO-DS MTT-corrected ratios.
(*) Denotes a statistically significant ($P < 0.01$) hemispheric asymmetry.

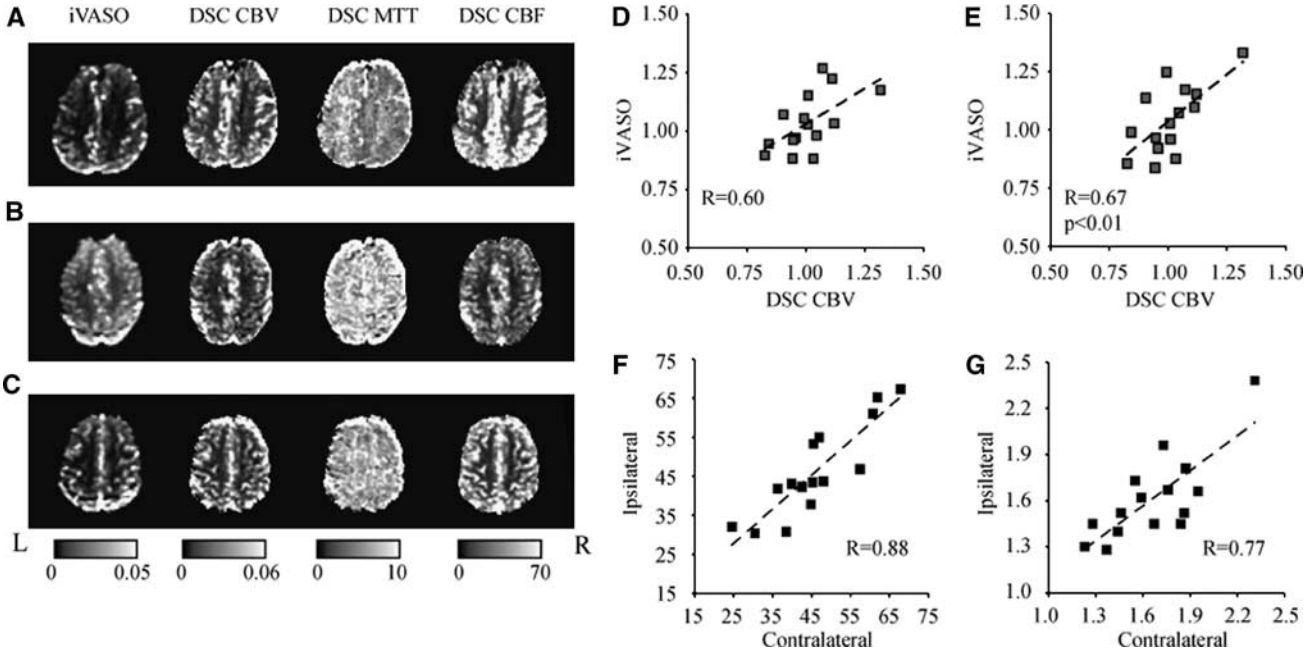

Figure 3 Representative iVASO difference images and DSC-computed CBV, MTT, and CBF maps for three representative patients: PT8 (**A**), PT16 (**B**), and PT6 (**C**); see Table 3 for patient details and symptoms. Contralateral:ipsilateral (to maximum ICA stenosis burden) iVASO ratios are plotted against DSC-CBV ratios before (**D**) and after (**E**) MTT correction. Ipsilateral versus contralateral CBF (**F**) and iVASO aCBV (**G**) reveal a higher hemispheric correlation for CBF ($R = 0.88$) compared with iVASO-measured aCBV ($R = 0.77$) in patients.

as may be expected for the limited burden present here. However, for patients with severe stenosis, aCBV is frequently, although not always, elevated contralateral to the maximum stenotic burden.

Figure 4 shows a summary of aCBV values. In Figure 4A, a histogram of all GM aCBV values for the healthy volunteer group is shown. There is a range of values with a peak at 1.0 to 1.5 mL/100 mL. The large spread in GM aCBV is likely attributable to different partial volume effects with small and large vessels, as well as possibly WM and CSF, and is the source of the large standard deviations in Tables 2 and 3. In Figure 4B, a box plot is shown summarizing the values for the healthy volunteers, patients with mild stenosis, and patients with severe stenosis. On average, aCBV values were not different between the control groups and any of the patient groups. However, a trend for significance was found between the contralateral hemisphere to maximum stenosis burden in severe stenosis patients and the healthy control group (Student's *t*-test; $P = 0.08$). However, though no aCBV asymmetry was found in any control, 7 of the 17 patients exhibited aCBV asymmetries, with 5 of these 7 patients having severe stenoses. These asymmetries were significant after accounting for MTT asymmetries.

Discussion

We show the feasibility of a new noninvasive MRI technique for measuring absolute aCBV. In this iVASO-DS approach, an image with and without inflowing blood signal is obtained, and the difference image is used to quantify aCBV in units of mL blood/100 mL parenchyma. Experiments were conducted at multiple inflow times, followed by an investigation of how aCBV in healthy volunteers compared with aCBV in patients with ICA steno-occlusive disease. First, simulations suggested that iVASO-DS contrast should vary linearly with aCBV (Figure 2B) for constant capillary arrival time, which was subsequently validated experimentally (Figure 2E). However, for 839 ms $<$ TI $<$ 1,064 ms, aCBV plateaus *in high SNR voxels*, reflecting the approximate range of capillary arrival times. Second, GM aCBV is $\sim$1.60 mL/100 mL in healthy volunteers and does not vary significantly ($P = 0.430$) between hemispheres. This finding was in contrast to patients with steno-occlusive disease, 41% of whom had asymmetric aCBV. In addition, symptomatic patients with severe stenosis had generally elevated GM aCBV (1.72 ± 0.18 mL/100 mL) relative to controls. Third, iVASO-DS hemispheric ratios corresponded with DSC-measured CBV ratios ($R = 0.60$), however this correlation improved ($R = 0.67$) and became significant ($P < 0.01$) when regional MTT asymmetries were taken into account (Figures 3D and 3E).

Arterial Cerebral Blood Volume

The aCBV values obtained are consistent with expected values from the literature, however varied

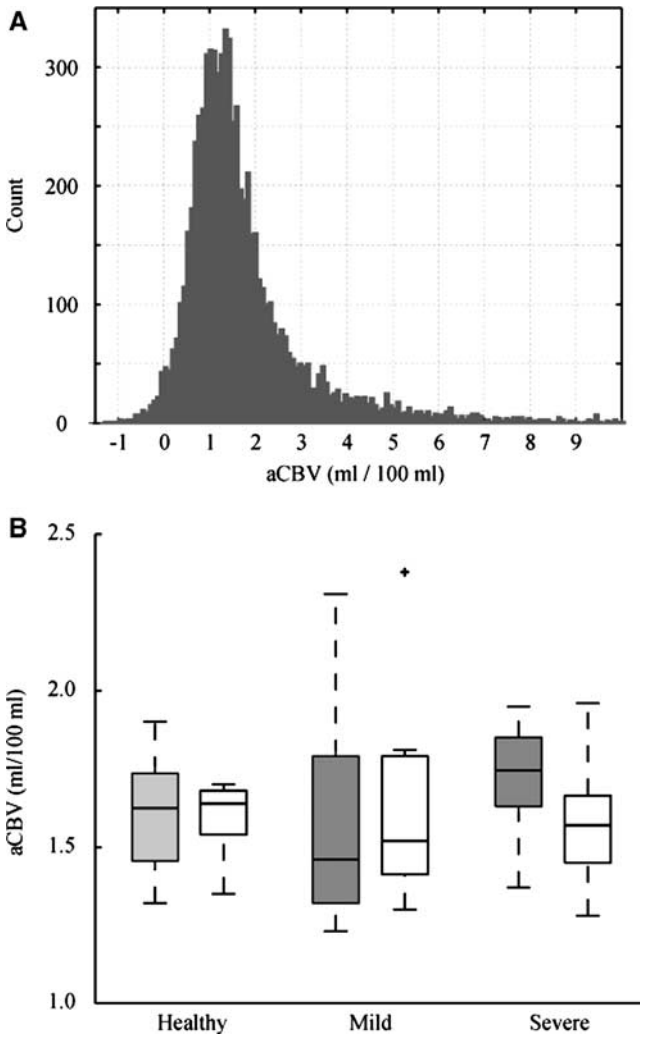

Figure 4 (**A**) Histogram of all GM aCBV values for the healthy control group. (**B**) Box plots of iVASO aCBV for the healthy control (left), mild stenosis (middle), and severe stenosis (right) volunteers. Gray is right in controls and contralateral to maximum stenosis burden in patients. White is left in controls and ipsilateral to maximum stenosis burden in patients. The central black line is the group median, the edges of the boxes are the 25th and 75th percentiles, the whiskers extend to the most extreme data points and any statistically significant outliers are plotted as black crosses.

over a physiologically expected range. Depending on the imaging modality used and region studied, total GM CBV is generally reported as 4.7 to 5.5 mL/100 mL (Giovacchini *et al*, 2002; Leenders *et al*, 1990; Lu *et al*, 2005). In addition, healthy precapillary CBV is commonly approximated as 20% to 30% of total CBV (An and Lin, 2002; van Zijl *et al*, 1998). This would lead to an expected GM aCBV of 0.94 to 1.65 mL/100 mL, which is in the range of the healthy aCBV measured here.

Recently, GM aCBV was estimated using ASL MRI and values were reported to be slightly lower: 0.93 ± 0.06 mL/100 mL (Petersen *et al*, 2006). This lower value, which is also approximately within the range of expected aCBV, could be due to differences in brain location or spatial resolution ($3.75 \times 3.75 \times 7\,mm^3$ versus $2.4 \times 2.4 \times 5\,mm^3$ used here). As larger voxels will partial volume with WM, which has a lower aCBV than GM, the larger voxel volume in the ASL study could account for some of the disparity. In addition, using MRI with modulation of tissue and vessel (MOTIVE) signals in isoflurane-anesthetized rats at 9.4 T, it was estimated that $aCBV = 1.1 \pm 0.5$ mL/100 mL in cerebral cortex (Kim and Kim, 2005). Although these results are slightly lower than the numbers we report here, they are within error of our results and of the physiologically expected range as well. Any remaining discrepancy could be explained by variations in spatial resolution, species, age, region of brain analyzed, and presence or absence of anesthesia.

Technical Considerations in iVASO-DS

We investigated the iVASO-DS contrast mechanism by qualitatively comparing iVASO-DS images acquired at multiple TIs with arterial TOF images and quantifying GM aCBV at each TI. It was found that aCBV varied linearly with TI in all GM voxels. However, when only voxels with high SNR were analyzed the aCBV reached a plateau for $TI \geq 839$ ms. This TI corresponds approximately to arterial transit times and indicates that at this inversion time, blood water may begin reaching the capillary bed. Once the bolus reaches the capillary bed, exchange between blood water protons and tissue water protons will influence the iVASO-DS map. However, we observed no such perfusion effects on the time scale of our TI experiments and therefore it is likely that exchange effects do not become significant until longer TI. Single TI ASL experiments are designed to capture these exchange effects for perfusion quantification and therefore use $TI \approx 1{,}500$ ms, which is much longer than the TI range here. On the basis of these results, TI = 839 to 1,064 ms is likely a promising window for aCBV quantification in iVASO-DS. In the case of patients with delayed capillary arrival times, a TI < capillary arrival time will lead to insufficient time for blood water to fill arteries + arterioles and an underestimation of aCBV. We have attempted to correct for this issue by incorporating MTT measures into our quantification procedure, however future work will benefit from individual subject capillary arrival time estimations, as can be achieved using the multi-TR/TI protocol from the methodological study here. Additionally, it is likely that sensitivity for microvasculature can be improved by incorporating bipolar flow-dephasing gradients with low *b*-value. Varying the magnitude of such gradients will result in sensitivity for different blood water velocities and therefore vessel diameters.

Measuring the capillary arrival time, which is defined here as the time for the labeled blood water bolus to move through the entire arterial + arteriolar

space to the capillary exchange site, is an important next step for regional quantification of aCBV using iVASO-DS. Here, we compare only left and right brain hemispheres, which are expected to have similar mean τ values in healthy subjects. We observed a MTT asymmetry in 5/17 patients, and account for this asymmetry in the iVASO-DS analysis. When aCBV values were corrected for hemispheric MTT differences, the iVASO-DS contrast correlated significantly with DSC-measured CBV contrast. However, two issues should be noted. First, MTT is not a measure of the capillary arrival time, but instead the mean time for the bolus to pass through tissue given an instantaneous arterial input function. In addition, iVASO-DS measures primarily precapillary CBV whereas DSC is sensitive to total CBV. Therefore, a one-to-one correlation may not be expected. However, the significant correlation between the two approaches does indicate that iVASO-DS is sensitive to a blood volume metric.

The model introduced here assumes that blood water outside the imaging slice is in a nulled steady state in the null experiments, whereas tissue and blood magnetization are both nonzero and unchanging in control experiments. Conditions may exist in which, especially at short TI, blood water enters the imaging slice during one TR and remains in the imaging slice in the next TR. Here, such blood water would experience a different RF history than the inflowing blood water (Figure 1B). This is likely only a problem at extremely short TI where blood water does not have sufficient time to leave the slice (5 mm) after excitation. In addition, for blood water remaining in the slice in subsequent TRs, the RF effects will be identical in control and null acquisitions (inversion + flip back). Such blood water will likely be traversing different vascular compartments, with the signal in the capillaries and veins in later TRs. This blood water will experience a new steady state in which the magnetization is identical in control and null acquisitions. Therefore, this signal should cancel during the subtraction procedure. Thus, the only blood water that is likely contributing to the iVASO-DS signal is the inflowing blood water, which is consistent with the hypothesis that iVASO-DS is primarily precapillary weighted.

The iVASO-DS implementation here was only a single-slice acquisition, which prevented a more systematic regional analysis of aCBV asymmetries. To acquire one slice, we performed 20 image acquisitions (10 control and 10 null), which took $\sim$36 secs. Therefore, a series of 10 slices ($\sim$50 mm coverage) could be obtained in 6 mins by performing each acquisition in a separate TR. A steno-occlusive disease study with larger volume coverage would be important for studying regional aCBV effects in different perfusion territories.

We only compartmentalize the voxel into extravascular GM tissue and blood, however even in the GM mask regions analyzed here, it is anticipated that some partial volume contributions from CSF and WM may be present. Future iVASO-DS models will likely benefit by inclusion of the contributions from these other compartments, and, by adapting existing multicompartment VASO models (Donahue *et al*, 2006) this should be possible. It has also been observed that when certain 3D readouts are used with traditional VASO imaging, such as 3D Gradient and Spin Echo (3D GRASE), a sensitivity improvement is found for nulling both blood water and CSF water simultaneously (Donahue *et al*, 2009*a*). This improvement is most noticeable with the 3D GRASE readout, and less so when a more typical 2D echo planar image readout is used, as is here. Future investigations should, however, be aimed at understanding contributions from CSF in the iVASO-DS signal, and also whether these contributions can be minimized with CSF signal nulling. This will be especially beneficial in patient studies where tissue atrophy may lead to additional CSF in the ROI. In this study, we observed no DWI lesions in the GM masks analyzed, although it is anticipated that in many patients, especially those with previous strokes, tissue atrophy, and lesions could lead to considerable partial volume effects and accurate aCBV quantification will need to account for this.

It should be noted that the iVASO-DS pulse sequence is similar to ASL as both sequences require RF manipulation of blood outside an imaging volume and a subtraction process. However, the contrast mechanism in iVASO-DS is fundamentally different than in ASL, as in iVASO-DS blood water is imaged before exchange with tissue water. This considerably simplifies certain aspects of the quantification process, but also reflects a different physiologic process (aCBV versus CBF). Therefore, though the pulse sequence is similar to an ASL sequence, the choice of TI = blood nulling generates a unique contrast. Moreover, it should be noted that iVASO-DS differs from a recently proposed ASL technique that measures CBF and aCBV (Petersen *et al*, 2006). aCBV is estimated by comparing images with and without blood water signal where bipolar gradients are used to dephase blood water signal as opposed to the VASO blood longitudinal magnetization nulling. This approach is also promising, however dephasing of blood water signal depends on the prescription of the gradient strength and direction. Similarly, with iVASO-DS, some blood water signal may not be nulled depending on which TI is used, and the corresponding blood water T_1 (which depends on hematocrit and oxygenation). We believe that both approaches may be useful sequences depending on the specific application and comparison studies would be of interest.

The SNR of iVASO-DS is expected to be comparable to ASL SNR. It is possible that iVASO-DS SNR may be slightly higher owing to the contrast mechanism being derived from blood water signal in vasculature, as opposed to smaller T_1 effects related to blood/tissue water exchange as is the case in ASL. However, a systematic comparison of SNR

will be required to demonstrate any disparity with certainty. Similarly, the iVASO-DS SNR is expected to be comparable to an alternative absolute CBV approach that uses a VASO acquisition before and after Gd injection (Lu *et al*, 2005). Here, Gd will shorten the intravascular T_1, leading to large intravascular signal in VASO after Gd injection, yet no intravascular signal in VASO before Gd injection. This approach benefits from the assumption that Gd will remain in the vasculature under normal conditions and therefore exchange effects are minimal, however has the disadvantage of requiring a contrast agent. We believe that the SNRs between ASL, iVASO-DS, and Gd-VASO are comparable, however additional work will be required to understand any potential discrepancy and how this discrepancy varies with TR/TI choice.

Finally, a slightly modified iVASO subtraction approach, similar to the approach presented here, has been suggested by Hua *et al*, and has been published in abstract form (Hua *et al*, 2009*b*), simultaneously with the abstract form of this study (Donahue *et al*, 2009*c*). Both studies should be useful for understanding the origin and feasibility of iVASO contrast.

Physiologic Observations and Clinical Potential

We found no significant difference in mean aCBV in right (1.60 ± 0.10 mL/100 mL) versus left (1.61 ± 0.20 mL/100 mL) hemispheres in healthy controls. However, we did find a large intervoxel variation in aCBV within hemisphere ROIs for individual subjects (Table 2; Figure 4A). This suggests that aCBV will vary significantly with voxel location and according to what extent the voxel partial volumes with large vessels.

The aCBV values from the healthy volunteers were compared against values in patients with steno-occlusive disease of the ICA. Unlike in the *healthy volunteer experiment*, aCBV was asymmetric in 41% of patients studied. This was most frequently on the side opposite to maximum stenosis burden and in patients with severe stenoses. Such an elevated aCBV is likely indicative of autoregulatory vasodilation in the presence of inadequate collateral circulation mechanisms. In patients with stenosis and no elevated aCBV, CBF may be maintained through collateral flow mechanisms. Given the reasonably small patient population recruited in this feasibility study ($n = 17$), as well as their varied clinical history, it is not possible to make any conclusive statements about aCBV in steno-occlusive disease. However, these data suggest that iVASO-DS contrast may be more asymmetric in patients relative to controls. Moreover, the quantified aCBV asymmetry is larger than the CBF asymmetries. Thus, aCBV may be an indicator of hemodynamic impairment in patients with steno-occlusive disease and aCBV adjustments may precede CBF adjustments in such patients. However, additional studies incorporating more patients, who are tracked over time, will be necessary to validate these hypotheses.

As most CBV measurements require contrast agent injection, it is difficult to track patient progression over time because of regulations on dose and general patient comfort issues. Therefore, noninvasive approaches would be useful for understanding the role of autoregulatory vasodilation on symptom progression, CBF, and reduced cerebral perfusion pressure. In addition, in acute stroke, aCBV may be an important parameter in identifying vessel compliance and ischemic tissue at risk of infarction. Patients with elevated aCBV may respond more positively to thrombolysis treatment than patients with reduced aCBV, and thus aCBV may provide a useful measure to complement standard DWI and DSC imaging. Measurement of aCBV may have a role in identifying asymptomatic patients with carotid atherosclerotic disease that are most likely to benefit from carotid endarterectomy. For instance, elevated aCBV may signify those patients with limited hemodynamic reserve and increased risk of stroke. This subgroup of asymptomatic patients may warrant the risk of carotid endarterectomy as they may gain the most benefit. This is an avenue for clinical research but at present an unanswered question.

Conclusions

We propose the new iVASO-DS method for generating absolute aCBV maps. The pulse sequence for iVASO-DS is similar to a combination of the ASL and iVASO sequences, and involves the subtraction of an image where the blood magnetization is nulled from an image where the blood magnetization is nonzero. It is found that this approach generates physiologically expected aCBV values over 839 ms $<$ TI $<$ 1,064 ms in high SNR voxels and corresponds with industry standard DSC-CBV imaging. In addition, aCBV was frequently elevated and more asymmetric in patients with severe steno-occlusive disease of the ICA, relative to controls. On the basis of these results, iVASO-DS may be a promising tool for probing autoregulatory aCBV and CBF compensation strategies, without the use of contrast agents, in patients with large vessel ischemic disease.

Acknowledgements

We are grateful to Steven Knight for experimental assistance and to all patients for their participation in this research study. This work was made possible by a grant from the Dunhill Medical Trust and the Oxford NIHR Biomedical Research Centre. This study was supported by the Dunhill Medical Trust, Heart and Stroke Foundation of Canada, National Institute of Health Research—Oxford Biomedical Research Centre.

Conflict of interest

The authors declare no conflict of interest.

References

An H, Lin W (2002) Cerebral venous and arterial blood volumes can be estimated separately in humans using magnetic resonance imaging. *Magn Reson Med* 48:583–8

Boysen G (1973) Cerebral hemodynamics in carotid surgery. *Acta Neurol Scand Suppl* 52:3–86

Derdeyn CP, Videen TO, Yundt KD, Fritsch SM, Carpenter DA, Grubb RL, Powers WJ (2002) Variability of cerebral blood volume and oxygen extraction: stages of cerebral haemodynamic impairment revisited. *Brain* 125:595–607

Donahue MJ, Blakeley JO, Zhou J, Pomper MG, Laterra J, van Zijl PC (2008) Evaluation of human brain tumor heterogeneity using multiple T1-based MRI signal weighting approaches. *Magn Reson Med* 59:336–44

Donahue MJ, Blicher JU, Ostergaard L, Feinberg DA, Macintosh BJ, Miller KL, Gunther M, Jezzard P (2009*a*) Cerebral blood flow, blood volume, and oxygen metabolism dynamics in human visual and motor cortex asmeasured by whole-brain multi-modal magnetic resonance imaging. *J Cereb Blood Flow Metab* 29:1856–66

Donahue MJ, Hua J, Pekar JJ, van Zijl PC (2009*b*) Effect of inflow of fresh blood on vascular-space-occupancy (VASO) contrast. *Magn Reson Med* 61:473–80

Donahue MJ, Lu H, Jones CK, Edden RA, Pekar JJ, van Zijl PC (2006) Theoretical and experimental investigation of the VASO contrast mechanism. *Magn Reson Med* 56:1261–73

Donahue MJ, Macintosh BJ, Sideso E, Bright M, Kennedy J, Handa A, Jezzard P (2009*c*) Absolute cerebral blood volume (CBV) quantification without contrast agents using inflow vascular-space-occupancy (iVASO) with dynamic subtraction. In: *International Society for Magnetic Resonance in Medicine*, Honolulu, Hawaii, Abs. 627

Donahue MJ, Piechnik SK, Tijssen R, Gallichan D, Miller KL, Jezzard P (2009*d*) A theoretical and experimental investigation of vascular-space-occupancy (VASO) blood nulling times: influence of hematocrit and oxygenation on null times and CBV quantification. In: *International Society for Magnetic Resonance in Medicine*, Honolulu, Hawaii

Giovacchini G, Chang MC, Channing MA, Toczek M, Mason A, Bokde AL, Connolly C, Vuong BK, Ma Y, Der MG, Doudet DJ, Herscovitch P, Eckelman WC, Rapoport SI, Carson RE (2002) Brain incorporation of [11C]arachidonic acid in young healthy humans measured with positron emission tomography. *J Cereb Blood Flow Metab* 22:1453–62

Griswold MA, Jakob PM, Heidemann RM, Nittka M, Jellus V, Wang J, Kiefer B, Haase A (2002) Generalized autocalibrating partially parallel acquisitions (GRAPPA). *Magn Reson Med* 47:1202–10

Gu H, Lu H, Ye FQ, Stein EA, Yang Y (2006) Noninvasive quantification of cerebral blood volume in humans during functional activation. *Neuroimage* 30:377–87

Hendrikse J, van Osch MJ, Rutgers DR, Bakker CJ, Kappelle LJ, Golay X, van der Grond J (2004) Internal carotid artery occlusion assessed at pulsed arterial spin-labeling perfusion MR imaging at multiple delay times. *Radiology* 233:899–904

Herscovitch P, Raichle ME (1985) What is the correct value for the brain–blood partition coefficient for water? *J Cereb Blood Flow Metab* 5:65–9

Hillman EM, Devor A, Bouchard MB, Dunn AK, Krauss GW, Skoch J, Bacskai BJ, Dale AM, Boas DA (2007) Depth-resolved optical imaging and microscopy of vascular compartment dynamics during somatosensory stimulation. *Neuroimage* 35:89–104

Hua J, Qin Q, Donahue MJ, Zhou J, Pekar JJ, van Zijl PC (2009*a*) Functional MRI using arteriolar cerebral blood volume changes. In: *The International Society for Magnetic Resonance in Medicine*, Honolulu, Hawaii, Abs. 12

Hua J, Qin Q, Pekar JJ, van Zijl P (2009*b*) Measuring absolute arteriolar cerebral blood volume (CBVa) in human brain gray matter (GM) without contrast agent. In: *International Society for Magnetic Resonance in Medicine*, Honolulu, Abs. 1533

Jenkinson M, Bannister P, Brady M, Smith S (2002) Improved optimization for the robust and accurate linear registration and motion correction of brain images. *Neuroimage* 17:825–41

Jin T, Kim SG (2006) Spatial dependence of CBV-fMRI: a comparison between VASO and contrast agent based methods. *Conf Proc IEEE Eng Med Biol Soc* 1:25–8

Kim T, Kim SG (2005) Quantification of cerebral arterial blood volume and cerebral blood flow using MRI with modulation of tissue and vessel (MOTIVE) signals. *Magn Reson Med* 54:333–42

Knutsson L, van Westen D, Petersen ET, Bloch KM, Holtas S, Stahlberg F, Wirestam R (2010) Absolute quantification of cerebral blood flow: correlation between dynamic susceptibility contrast MRI and model-free arterial spin labeling. *Magn Reson Imaging* 28:1–7

Leenders KL, Perani D, Lammertsma AA, Heather JD, Buckingham P, Healy MJ, Gibbs JM, Wise RJ, Hatazawa J, Herold S *et al* (1990) Cerebral blood flow, blood volume and oxygen utilization. Normalvalues and effect of age. *Brain* 113(Pt 1):27–47

Lu H, Clingman C, Golay X, van Zijl PC (2004) Determining the longitudinal relaxation time (T1) of blood at 3.0 Tesla. *Magn Reson Med* 52:679–82

Lu H, Golay X, Pekar JJ, Van Zijl PC (2003) Functional magnetic resonance imaging based on changes in vascular space occupancy. *Magn Reson Med* 50:263–74

Lu H, Law M, Johnson G, Ge Y, van Zijl PC, Helpern JA (2005) Novel approach to the measurement of absolute cerebral blood volume using vascular-space-occupancy magnetic resonance imaging. *Magn Reson Med* 54:1403–11

Nichols TE, Holmes AP (2002) Nonparametric permutation tests for functional neuroimaging: a primer with examples. *Hum Brain Mapp* 15:1–25

Ostergaard L, Smith DF, Vestergaard-Poulsen P, Hansen SB, Gee AD, Gjedde A, Gyldensted C (1998) Absolute cerebral blood flow and blood volume measured by magnetic resonance imaging bolus tracking: comparison with positron emission tomography values. *J Cereb Blood Flow Metab* 18:425–32

Petersen ET, Lim T, Golay X (2006) Model-free arterial spin labeling quantification approach for perfusion MRI. *Magn Reson Med* 55:219–32

Petersen ET, Mouridsen K, Golay X (2009) The QUASAR reproducibility study, Part II: Results from a multi

center Arterial Spin Labeling test-retest Study. *Neuroimage* 49:104–13

Powers WJ, Raichle ME (1985) Positron emission tomography and its application to the study of cerebrovascular disease in man. *Stroke* 16:361–76

Rapela CE, Green HD (1964) Autoregulation of canine cerebral blood flow. *Circ Res* 15(Suppl):205–12

Sakai F, Nakazawa K, Tazaki Y, Ishii K, Hino H, Igarashi H, Kanda T (1985) Regional cerebral blood volume and hematocrit measured in normalhuman volunteers by single-photon emission computed tomography. *J Cereb Blood Flow Metab* 5:207–13

Schumann P, Touzani O, Young AR, Morello R, Baron JC, MacKenzie ET (1998) Evaluation of the ratio of cerebral blood flow to cerebral blood volume asan index of local cerebral perfusion pressure. *Brain* 121(Pt 7):1369–79

Scouten A, Constable RT (2008) VASO-based calculations of CBV change: accounting for the dynamic CSF volume. *Magn Reson Med* 59:308–15

Stefanovic B, Pike GB (2005) Venous refocusing for volume estimation: VERVE functional magnetic resonance imaging. *Magn Reson Med* 53:339–47

Steiger HJ, Aaslid R, Stooss R (1993) Dynamic computed tomographic imaging of regional cerebral blood flow and blood volume. A clinical pilot study. *Stroke* 24:591–7

Uh J, Lewis-Amezcua K, Martin-Cook K, Cheng Y, Weiner M, Diaz-Arrastia R, Devous M Sr, Shen D, Lu H (2009) Cerebral blood volume in Alzheimer's disease and correlation with tissue structural integrity. *Neurobiol Aging*; 4 February 2009 (e-pub ahead of print)

van Zijl PC, Eleff SM, Ulatowski JA, Oja JM, Ulug AM, Traystman RJ, Kauppinen RA (1998) Quantitative assessment of blood flow, blood volume and blood oxygenation effects in functional magnetic resonance imaging. *Nat Med* 4:159–67

Villringer A, Rosen BR, Belliveau JW, Ackerman JL, Lauffer RB, Buxton RB, Chao YS, Wedeen VJ, Brady TJ (1988) Dynamic imaging with lanthanide chelates in normal-brain: contrast due tomagnetic susceptibility effects. *Magn Reson Med* 6:164–74

Wintermark M, Albers GW, Alexandrov AV, Alger JR, Bammer R, Baron JC, Davis S, Demaerschalk BM, Derdeyn CP, Donnan GA, Eastwood JD, Fiebach JB, Fisher M, Furie KL, Goldmakher GV, Hacke W, Kidwell CS, Kloska SP, Kohrmann M, Koroshetz W, Lee TY, Lees KR, Lev MH, Liebeskind DS, Ostergaard L, Powers WJ, Provenzale J, Schellinger P, Silbergleit R, Sorensen AG, Wardlaw J, Wu O, Warach S (2008) Acute stroke imaging research roadmap. *AJNR Am J Neuroradiol* 29:e23–30

Wu WC, Buxton RB, Wong EC (2007) Vascular space occupancy weighted imaging with control of residual blood signal and higher contrast-to-noise ratio. *IEEE Trans Med Imaging* 26:1319–27

Zaharchuk G, Mandeville JB, Bogdanov AA, Jr, Weissleder R, Rosen BR, Marota JJ (1999) Cerebrovascular dynamics of autoregulation and hypoperfusion. An MRI study of CBF and changes in total and microvascular cerebral blood volume during hemorrhagic hypotension. *Stroke* 30:2197–204; discussion 2204–2195

Zhao JM, Clingman CS, Narvainen MJ, Kauppinen RA, van Zijl PC (2007) Oxygenation and hematocrit dependence of transverse relaxation rates of blood at 3T. *Magn Reson Med* 58:592–7